ACS OMEGA

Open Access

http://pubs.acs.org/journal/acsodf

Article

Label-free Detection of Urine Extracellular Vesicles from Duchenne Muscular Dystrophy Patients Using Surface-Enhanced Raman Spectroscopy Combined with Machine Learning Models

Archana Rajavel, Jayasree Kumar,[#] Narayanan Essakipillai,[#] Ramajayam Anbazhagan, Rajapandiyan Panneerselvam, Jayashree Ramakrishnan, Viswanathan Venkataraman, and Raja Natesan Sella*

Cite This: *ACS Omega* 2025, 10, 16874−16883

Read Online

ACCESS | Metrics & More | Article Recommendations | Supporting Information

ABSTRACT: Duchenne muscular dystrophy (DMD) is a neuromuscular disease that affects males in the pediatric age group. Currently, there is no painless, cost-effective prognostic method available to monitor DMD progression. The main hypothesis of this study was that the biochemical composition of extracellular vesicles (EVs) isolated from the urine of DMD patients can be distinctly differentiated from that of healthy controls using surface-enhanced Raman Spectroscopy (SERS) combined with machine learning models. This differentiation is expected to provide a noninvasive, rapid, and accurate diagnostic tool for the early detection, staging, and monitoring of DMD by identifying the molecular signatures captured by SERS and leveraging the analytical power of machine learning algorithms. We collected fasting morning urine samples from 52 DMD patients and 17 healthy controls and isolated EVs using a Total Exosome Isolation kit. The SERS substrates are prepared using silver nanoparticles, which were employed to capture the molecular fingerprints of the EVs with uniformity and reproducibility, achieving relative standard deviation values of 7.3% and 8.9%. We observed alterations in phenylalanine and α-helical proteins in patients with DMD compared to controls. These spectral data were analyzed using PCA, Support Vector Machines, and k-Nearest Neighbor (KNN) algorithms to identify distinct patterns and stage DMD based on biochemical composition. Our integrated approach demonstrated 60% sensitivity and 100% specificity in distinguishing DMD patients from healthy controls, highlighting the potential of SERS and KNN for noninvasive, accurate, and rapid diagnosis of DMD. This method offers a promising avenue for early detection and personalized treatment strategies, ultimately improving patient outcomes and quality of life.

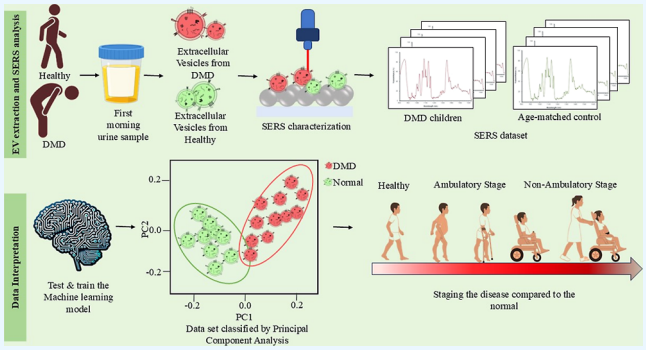

INTRODUCTION

Duchenne muscular dystrophy (DMD) is one of the severe forms of muscular dystrophy which is a progressive genetic disorder characterized by the eventual loss of mobility, degeneration of muscle tissue, and leads to muscle weakness.[1,2] It primarily affects males aged 2−5 years, with symptoms typically manifesting in early childhood. Mutations in dystrophin, an essential protein for the structural integrity of muscle fibers, cause this rare disorder. Muscle cells begin to degenerate as they are easily vulnerable to damage due to a lack of dystrophin. The clinical presentation of DMD includes delayed motor milestones, difficulty in walking, muscle weakness, and eventual loss of ambulation, usually in the teenage years. Additionally, individuals with DMD may experience complications, such as cardiomyopathy, respiratory insufficiency, and skeletal deformities, significantly affecting their quality of life and shortening their life expectancy.[3]

Despite the significant clinical importance of early diagnosis, traditional diagnostic methods[4−7] for DMD, such as genetic testing and muscle biopsy,[4] may be invasive, require lengthy processing time,[8] and are costly. Therefore, there is a critical need for rapid, noninvasive, and accurate diagnostic tools for DMD that can facilitate early detection and intervention, ultimately improving outcomes for affected individuals and their families.[9] Biomarkers for neuromuscular diseases can enhance quality of life, enable early intervention, and improve clinical trials.[1,10−12] These diseases are prevalent and

Received: January 28, 2025
Revised: March 1, 2025
Accepted: March 6, 2025
Published: March 24, 2025

https://doi.org/10.1021/acsomega.5c00838
ACS Omega 2025, 10, 16874−16883

expensive, resulting in high mortality and significant financial burdens on patients.[13]

Membrane-bound vesicles popularly known as extracellular vesicles (EVs) communicate between different cells where bioactive molecules such as proteins, lipids, and nucleic acids are released into the extracellular environment.[14,15] In the emerging field of science, EVs are now a potential biomarker for various diseases, more importantly neurodegenerative disorders and cancer.[16−19] Their ability to reflect the molecular signatures of their parent cells makes them attractive candidates for biomarker discovery and disease diagnosis.[20−22] They are used in a noninvasive sampling method that is easily accessible from bodily fluids, such as blood, urine, and saliva, eliminating the need for invasive tissue biopsies.[23−26] EVs are highly stable, surrounded by lipid bilayers, and maintain their integrity under challenging conditions.[27] They are the reservoir of biomarkers and reflect the disease state.[20,28,29]

Advances in EV isolation techniques and analytical methods have facilitated the identification and characterization of EV-associated biomarkers. The current analytical techniques for profiling the composition of EV including Fourier transform infrared spectroscopy (FTIR)[30−33] and Matrix-Assisted Laser Desorption/Ionization Time-of-Flight Mass Spectrometry (MALDI-TOF MS)[34−36] offer valuable insights but have notable limitations. FTIR provides general molecular information by detecting vibrations of biomolecules, but its sensitivity is low, making it less effective for detecting low-abundance molecules within EVs. Similarly, while MALDI-TOF MS excels in identifying and quantifying proteins and lipids based on mass-to-charge ratios, it is destructive.[37,38] Additionally, both techniques struggle with the real-time analysis of liquid samples, making them less adaptable for clinical applications involving biofluids. In contrast, Surface-enhanced Raman spectroscopy (SERS) provides a wide range of molecular fingerprints of multiple biomolecules, including proteins, lipids, and nucleic acids, with minimal sample preparation.[39,40] Importantly, SERS is nondestructive, highly sensitive, and compatible with the real-time analysis of liquid biofluids such as urine and plasma, making it a versatile tool for comprehensive EV profiling.[41−43] This combination of sensitivity, molecular specificity, and practical ease makes SERS a powerful method for studying EVs, especially in the context of disease biomarker discovery.[44−46]

Machine learning is a branch of artificial intelligence that uses multiple algorithms, such as Convolutional Neural Networks (CNN), k-Nearest Neighbor (KNN), partial least squares (PLS) Regression, Random Forests, Linear Discriminant Analysis (LDA), and Support Vector Machines (SVM), to analyze small to large data sets and reduce complexity. SERS spectra, which consist of numerous intensity values across various Raman shifts, often exhibit nonlinear relationships and are prone to noise.[47] These algorithms help to identify patterns, classify samples, and optimize predictive models. The integration of machine learning with SERS has gained popularity, with researchers using LDA for SARS-CoV-2,[48] random forest for lipid signal analysis,[49] and CNN for early cancer detection.[50]

Our proof-of-concept study uses PCA, SVM, and KNN algorithms to analyze the SERS data, detect urine EVs without labeling, and predict the stages of DMD patients. This method enhances sensitivity and specificity by providing detailed biochemical profiling and identifying disease-associated patterns. Machine learning can also identify molecular signatures indicative of DMD pathogenesis, enabling automated analysis and personalized treatment management. This proof-of-concept study shows the results of SERS spectra from the urine extracellular vesicles (UEVs) of stratified DMD patients without labeling using machine learning.

RESULTS AND DISCUSSION

Characteristics of Extracted Urine EVs by Transmission Electron Microscopy, Nanoparticle Tracking Analysis, and Western Blotting Analysis. The morphology and size of EVs isolated from the urine of healthy individuals were characterized by high-resolution transmission electron microscopy (HR-TEM), nanoparticle tracking analysis (NTA), and Western Blotting. HR-TEM images confirmed the presence of EVs, showing a heterogeneous size distribution and spherical shape with preserved lipid membrane integrity (Figure 1a). NTA revealed that the size of UEVs from healthy

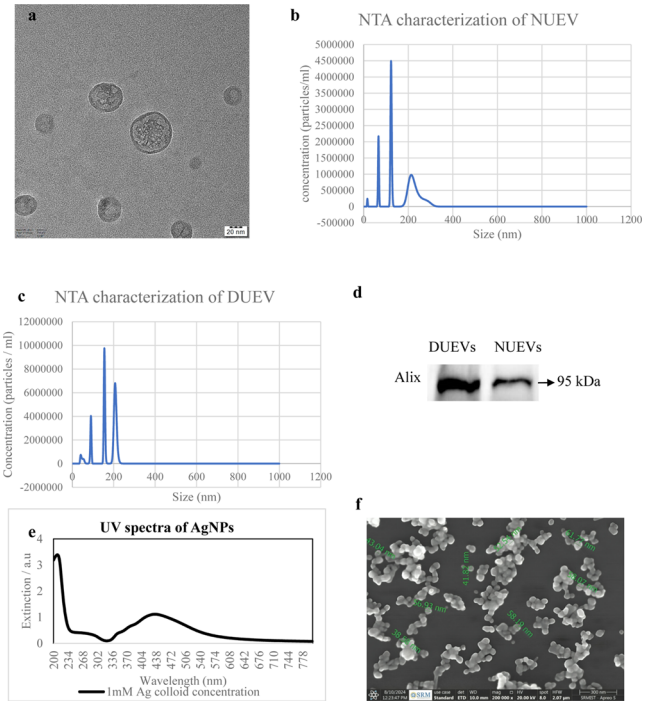

Figure 1. Biophysical and Molecular characterization of UEVs (a) High-Resolution TEM micrograph of a heterogeneous population of UEVs exhibiting characteristic spherical morphology and surrounded by a single membrane. Image captured at a magnification of 80,000× and an accelerating voltage of 200 kV. (b) Size distribution and particle concentration of UEVs of DMD patients and healthy controls using NTA. The mean size of EVs from healthy controls is 168 nm with a concentration of 2.2×10^7 particles/mL. (c) In contrast, DMD-derived EVs have a mean size of 174.1 nm and a concentration of 9.9×10^7 particles/mL. The size and number of EVs showed significant difference between DMD patients and healthy individuals. (d) Western blot analysis of UEVs for the presence of Alix (95 kDa). The results show a distinct band corresponding to Alix, indicating the successful isolation of EVs from the samples. (e) UV−visible spectra of Silver (Ag) colloids prepared for SERS Analysis. The UV−visible spectra of the Ag colloids exhibit a distinct peak around 430 nm, indicative of spherical silver nanoparticles. (f) A high magnification scanning electron microscopy image highlighting the spherical shape and size distribution of the AgNPs, which range from 40 to 60 nm. This size range is ideal for enhancing the Raman signal due to the localized surface plasmon resonance (LSPR) effect.

https://doi.org/10.1021/acsomega.5c00838
ACS Omega 2025, 10, 16874−16883

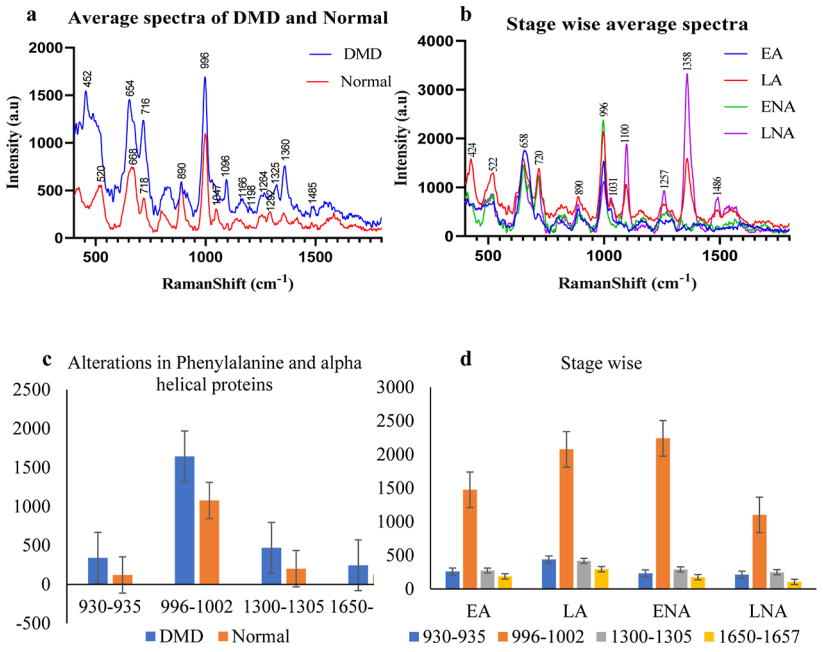

Figure 2. (a) Line graph depicting the average SERS spectra of DMD patients and age-matched controls. The prominent peaks indicate significant biochemical differences between the two groups. (b) Average SERS spectra of four stages of DMD patients. (c) The bar chart illustrates the significant increase in phenylalanine levels and decrease in alpha spectral protein levels in UEVs from DMD patients. (d) The chart depicts the levels of phenylalanine and alpha spectral proteins in UEVs from patients at four different stages of DMD: EA—Early Ambulatory, LA—Late Ambulatory, ENA—Early Non-Ambulatory, and LNA—Late Non-Ambulatory.

subjects ranged from 20 to 250 nm, with an average size of 168 nm and a concentration of 2.2×10^7 particles/mL in a normal sample (Figure 1b). In contrast, EVs from DMD patients had a slightly larger average size of 174.1 nm and a higher concentration of 9.9×10^7 particles/mL (Figure 1c). These findings highlight significant differences in the biophysical characteristics like size and number of EVs in a sample between healthy individuals and DMD patients.[51] The Western blot analysis shows that Alix is present in the UEV samples, confirming that the EVs were successfully isolated (Figure 1d). Alix, a protein important for the formation and sorting of EVs, is a reliable marker for identifying them. The clear band at around 95 kDa indicates that the EVs retain their typical protein composition after isolation.[51]

UV Spectroscopy and HR-SEM Characterization of the Prepared SERS Substrate. The synthesized silver colloids exhibited a distinct peak at 430 nm in the UV spectrum. These nanoparticles have appropriate optical properties for SERS analysis with a size range of 40−60 nm and a predominantly spherical shape. An equal volume of nanoparticles and Urine EVs was prepared for SERS analysis, with glass slides wrapped in aluminum foil for substrate preparation. HR-SEM validation confirmed the uniform distribution and proper adhesion of the nanoparticles. The spherical silver nanoparticles, with their size range of 40−60 nm, are ideal for enhancing the Raman signal due to the localized surface plasmon resonance effect shown in (Figure 1e,f).[52]

Presentation of Spectral Data from DMD Patients and Healthy Controls. Distinct SERS peaks represent proteins, lipids, and nucleic acids based on the vibrational mode. Urine-EVs carry the molecular information that reflects the pathophysiological processes in DMD. The molecular composition of UEVs at different stages of DMD patients is characterized by muscle weakness, fibrosis, and inflammation.[2,53] Urine EVs' protein and lipid cargo levels differ from the early ambulatory to the late nonambulatory stage. The release of muscle-specific cargoes such as myosin, tropomyosin, actin, and type 1 collagen in circulation, and excretion of DMD patients was analyzed using SERS. Maria Plesia's group studied the muscle, bone, and blood in vitro models of ALS and DMD using Raman spectroscopy studied corresponding muscle protein peaks are shown in Table S1 with the vibrational mode and peak assignments.[54] We studied the significant spectral patterns of UEVs from DMD patients and age-matched controls.

The average SERS spectral analysis demonstrated significant biochemical alterations in the disease states of DMD patients compared with age-matched healthy controls (Figure 3a). Notably, there was an increased concentration of collagen (654 cm^{-1}), nucleic acids (716 cm^{-1}), phenylalanine breathing mode (996 cm^{-1}), tryptophan (1360 cm^{-1}), lipids and carbohydrates (1096 cm^{-1}), and C−H bending of tyrosine, phenylalanine, and proteins (1167 cm^{-1}). These elevations suggest increased extracellular matrix (ECM) remodeling, higher cellular turnover or damage, altered protein metabolism, increased muscle protein breakdown, and disrupted metabolic processes and protein homeostasis in DMD patients. Conversely, the spectra indicated decreased concentrations of phosphatidylinositol (520 cm^{-1}), galactosamine/glutathione (890 cm^{-1}), proline (1047 cm^{-1}), and alpha spectral helix proteins (1264 cm^{-1}) in children with DMD. These reductions suggest disrupted phospholipid metabolism, oxidative stress, impaired detoxification mechanisms, altered collagen synthesis, and changes in protein secondary structure associated with muscle degradation.

Figure 2a,b shows the average SERS spectra of four different stages of DMD, highlighting the biochemical changes at each stage. In the early ambulatory stage, there was an increased concentration of collagen type I (658 cm^{-1}) and Phenylalanine

https://doi.org/10.1021/acsomega.5c00838
ACS Omega 2025, 10, 16874−16883

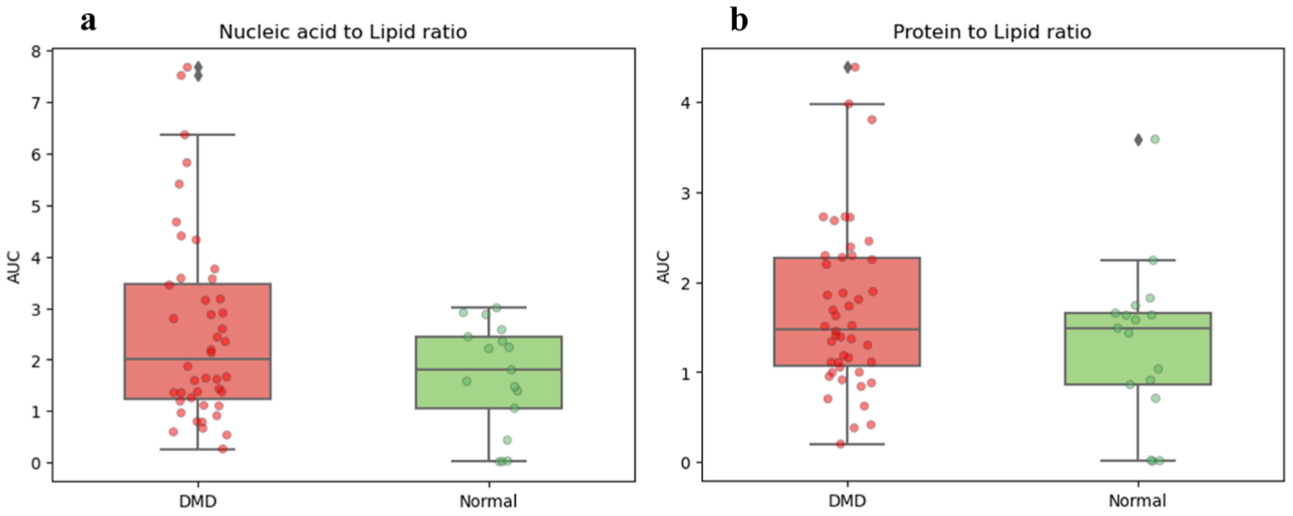

Figure 3. (a) Nucleic acid to lipid ratio in UEVs from DMD patients compared to age-matched healthy controls. (b) Protein to lipid ratio in UEVs from DMD patients and age-matched controls.

(996 cm^{-1}), and a decreased concentration of proline (1051 cm^{-1}) compared to the age-matched control group. In the late ambulatory stage, elevated levels of phosphatidylinositol (520 cm^{-1}), collagen (648 cm^{-1}), nucleic acids (718 cm^{-1}), phenylalanine (996 cm^{-1}), Lipids and carbohydrates (1097 cm^{-1}), Amide III region of α-helical proteins (1257 cm^{-1}), tryptophan (1360 cm^{-1}) are observed, along with reduced levels of proline (1047 cm^{-1}). As DMD progressed from the ambulatory stage to the wheelchair-bound (early non-ambulatory) stage, the levels of phosphatidylinositol (522 cm^{-1}), collagen (652 cm^{-1}), nucleic acids (715 cm^{-1}), phenylalanine (998 cm^{-1}), tyrosine, phenylalanine, proteins (1169 cm^{-1}), amide III region of α-helical proteins (1264 cm^{-1}), and tryptophan level (1356 cm^{-1}) decreased than controls. In the late nonambulatory stages, DMD children lose their muscle mass and have complications in heart and lung function. The levels of lipids and carbohydrates (1100 cm^{-1}), the amide III region of α-helical proteins (1257 cm^{-1}), and tryptophan (1358 cm^{-1}) drastically increased. The levels of collagen (650 cm^{-1}), galactosamine/glutathione (890 cm^{-1}), and phenylalanine (996 cm^{-1} and, 1027 cm^{-1}) were comparable to those in the control groups.

In the average spectra shown in Figure 2a,b, the peak (520 cm^{-1}) represents phosphatidylinositol, which regulates lipid metabolism, membrane trafficking, and signaling in eukaryotic cells. Repressing phosphatidylinositol transfer protein alpha modulates pathological signaling cascades that exacerbate muscle damage and inflammation. It helps stabilize the cell membranes, reduce muscle degeneration, and improve muscle function in DMD patients.[55] One of the pathological features of DMD is increased muscle stiffness, owing to intramuscular fibrosis. The abnormal buildup of ECM components, particularly collagens I, IV, and VI, disrupts normal muscle function. These collagens communicate with integrins to mediate Cell-ECM interactions.[56−58] The ongoing cycles of muscle damage and repair in DMD patients lead to chronic inflammation and stimulate fibroblasts to produce excessive collagen. Figure 3a shows that the level of collagen (650 cm^{-1}) notably increased in DMD patients. Furthermore, our results highlight that collagen deposition increases in the late ambulatory stage. The deposition of collagen increases muscle stiffness and restricts the ability of the diaphragm to contract and expand effectively. As fibrosis progresses, the diaphragm's reduced mobility can lead to respiratory insufficiency, which is one of the leading causes of death in DMD patients.[59,60] Normally, dystrophin helps to stabilize and protect muscle fibers during contraction and relaxation. In DMD, dysfunctional dystrophin renders the muscle cell membrane more fragile and susceptible to damage. This damage leads to an increased leakage of adenine nucleotides from the muscle cells to the extracellular space. The loss of adenine nucleotides necessitates rapid replenishment, resulting in accelerated turnover as the cells attempt to maintain adequate adenosine 5′-triphosphate (ATP) levels to support normal muscle function and repair.[61−64] Researchers aimed to increase ATP synthesis that could benefit DMD patients' treatments such as metabolic supplements, pharmacological agents, gene therapy, exercise, and physical therapy. Adenine base editing is a CRISPR-Cas 9-based approach[65] to treat DMD that directly converts adenine (A) to guanine (G) at a targeted site. They are specific to nonsense mutation and derived from induced pluripotent stem cells into cardiomyocytes of DMD patients restoring the full-length dystrophin.[65,66] Glutathione (890 cm^{-1}) is the antioxidant detected higher in the muscles of adult DMD patients than in juveniles.[67] There is reorganization of the sulfation pattern of chondroitin sulfate disaccharide units in the muscles of patients with DMD, particularly the increased 4-O- sulfation of *N*-acetyl-galactosamine residues. This could lead to the upregulation of chondroitin 4-sulfotransferase-1 and could serve as a therapeutic target in DMD.[68] Phenylalanine (PA) is an essential amino acid for the proper functioning of the brain and nervous system provided by a diet. Elevated plasma PA levels are closely related to the processes of cardiac aging[69] and the rate of muscle protein synthesis and breakdown.[70] In the early and late stages of mdx groups, the rate of synthesis and breakdown was significantly higher than in the control mice groups. A more negative net balance indicates that muscle protein breakdown exceeds synthesis, which leads to muscle wasting or degeneration. The PA utilization of the body can be an indicator of muscle protein turnover.[70] PA flux is strongly associated with changes in the net balance of muscle proteins. The whole-body rate of PA disposal in the postabsorptive state is directly proportional to the hydroxylated tyrosine and protein lysis. Muscle tissue lacks

https://doi.org/10.1021/acsomega.5c00838
ACS Omega 2025, 10, 16874−16883

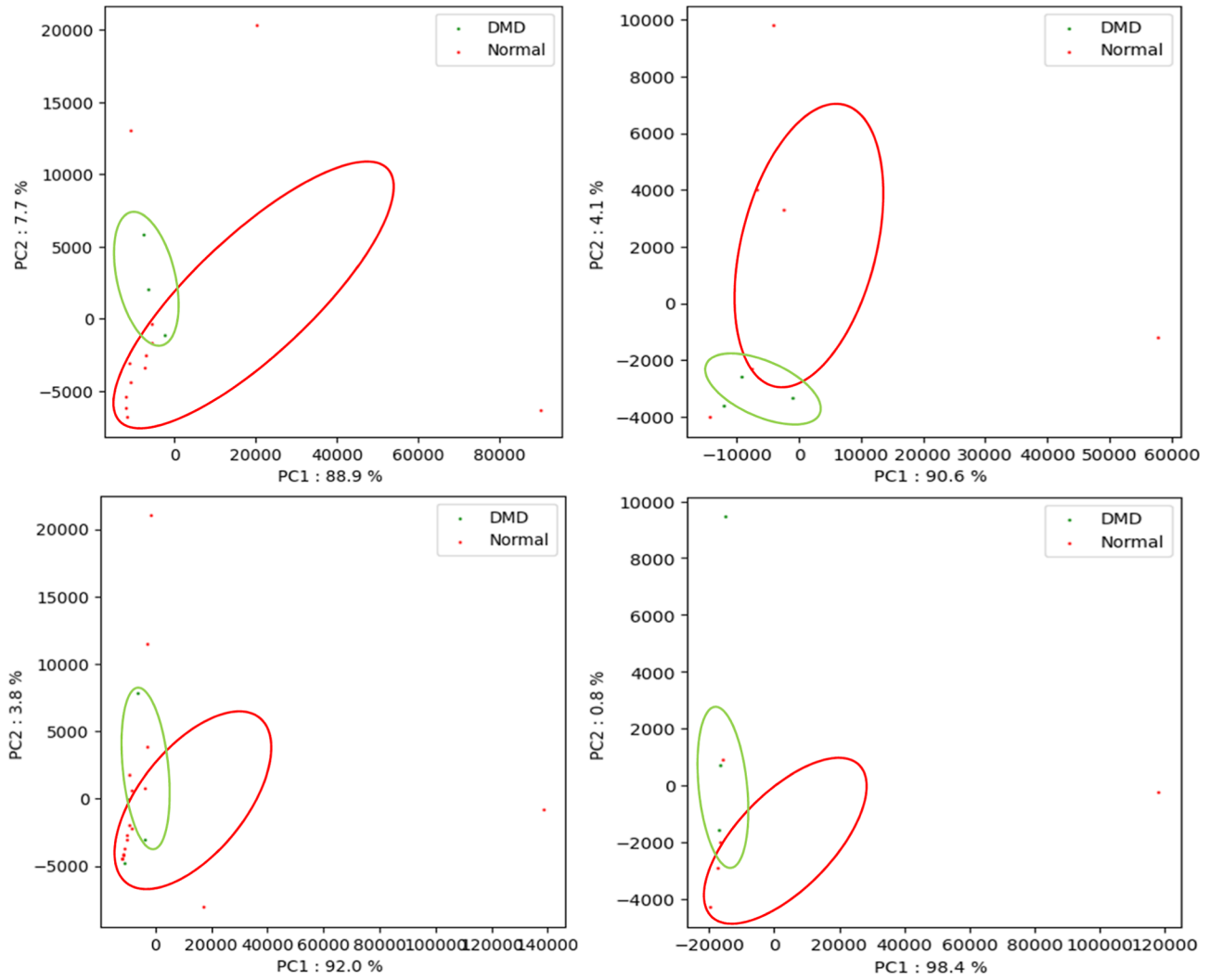

Figure 4. The PCA plot shows distinct clusters representing different stages of DMD (Early ambulatory to Late Non-Ambulatory) and the control group, indicating variations in UEVs cargo profiles corresponding to disease progression.

the phenylalanine hydroxylase enzyme that helps to hydroxylate tyrosine. The use of PA tracers in DMD provides a powerful tool for monitoring muscle breakdown and synthesis. This can significantly contribute to improving the management and outcomes of patients with DMD.[70]

The intensity of the phenylalanine (996 cm^{-1}) and alpha spectral protein peaks shows significant differences in all stages of DMD compared to the age-matched control groups[69,70] (Figure 2c). The chart shows the metabolic and proteomic changes associated with DMD progression, reflecting the impact of the disease on muscle protein turnover and composition. Alterations in phosphatidylinositol, lipid, carbohydrates, and nucleic acid regions have been shown in all stages of DMD compared with control groups (Figure 2d).[71] During the progression of DMD, the α-helical proteins are reduced or lost in muscle degeneration.[72]

In statistical analysis, the ratio of nucleic acids and proteins to lipids from UEVs showed a significant difference in DMD compared with that of age-matched controls (Figure 3a). The data reveal a significant increase in the nucleic acid to lipid ratio in the EVs from DMD patients, indicating altered biochemical composition and potential disruptions in nucleic acid metabolism associated with the disease. In Figure 3b, the box plot shows a marked elevation in the protein-to-lipid ratio in the EVs from DMD patients, suggesting significant changes in EVs' protein composition, which may reflect muscle degeneration and increased protein turnover characteristic of the disease.

The statistical analysis of the peaks in our data (Table S3) compared with prominent peaks is already reported by previous studies at significance $P < 0.01$ except for the 870–950 cm^{-1} peak range.

Performance Metrics of Machine Learning Models for DMD Classification. We performed a 5-fold cross-validation and constructed a confusion matrix to evaluate our proposed ML model using PCA, SVM, and K-NN algorithms for classifying cases and controls. Initially, 80% of the data set were used to train the model, and the predictive performance of the model was assessed using the remaining 20% of the data set. Our ML model has been developed to effectively capture the small molecular patterns in SERS spectra from UEVs, facilitating precise diagnosis, staging, and monitoring of DMD. As shown in Figure 4, PCA of SERS spectral patterns of the four stages of DMD, from ambulation to nonambulation stages, shows PC1 above 85% of the variance and PC2 below 8%. The K-NN model accurately classifies the small data set and effectively differentiates between the DMD and control groups. The K-NN model predicts the DMD and control

https://doi.org/10.1021/acsomega.5c00838
ACS Omega 2025, 10, 16874−16883

groups more accurately, without Type II errors, than the SVM model. The values of accuracy, sensitivity, specificity, precision, and AUROC are shown in (Table 1).

Table 1. Performance Metrics of KNN and SVM Machine Learning Models

ML algorithm	accuracy (%)	sensitivity (%)	specificity (%)	precision (%)	AUROC
KNN	85.71	60.00	100	100	0.73
SVM	64.29	60.00	66.67	50.00	0.20

CONCLUSIONS

Our SERS ML approach can help monitor muscle wasting or degeneration in both juvenile and adult DMD patients without labeling. This simple and quick procedure performed within 1 h from EV extraction to ML prediction is amenable to incorporation into clinical settings. The KNN predicts the DMD with an accuracy of 85.71% and the ambulation status with an accuracy of 64.29%, respectively. This precision is crucial for timely intervention and personalized treatment strategies, ultimately improving patient outcomes. Moreover, the noninvasive nature of this approach makes it a more patient-friendly option than traditional biopsy methods for other muscular dystrophies.

MATERIALS AND METHODS

Materials. All chemicals and solvents were commercially available and were used directly. The Total Exosome Isolation (TEI) kit was purchased from Invitrogen, USA, Tris-hydrochloride (Tris−HCl), sodium deoxycholate, Nonidet P-40, Sodium chloride (NaCl), Ethylenediamine tetraacetic acid (EDTA), PMSF protease inhibitors, and bovine serum albumin (BSA) were acquired from Himedia Laboratories (Mumbai, MH, India). Bicinchoninic Acid was procured from Thermo Fisher and Tween-20 and a protease inhibitor cocktail were obtained from Sigma- Aldrich (St. Louis, MO, USA). Nitrocellulose membranes were purchased from BioRad (Hercules, CA, USA) and Alix (3A9) mouse monoclonal antibody (mAb) was obtained from Cell Signaling Technology, Inc. (Danvers, MA, USA).

Trisodium citrate dihydrate ($Na_3C_6H_5O_7{\cdot}2H_2O$) and Silver nitrate ($AgNO_3$) were purchased from Scharlau Chemicals and Sigma-Aldrich. Methanol (99.9%) was obtained from Thermo Fisher Scientific, USA. Blue star microscope glass slides (3 × 1) with polished edges were supplied by Siscon, India. To prepare all aqueous solutions, reagent grade chemicals and (Millipore Milli-Q system) deionized water with a resistivity of 18.5 MΩ cm were used.

METHODOLOGY

Sample Collection and EV Isolation from Urine. We collected 30 mL of morning urine from fasting individuals in collection tubes containing PMSF protease inhibitors. The study included 52 individuals who had been diagnosed with DMD and 17 healthy juvenile subjects ranging in age from 5 to 20 years. Approval for the study was obtained from the Institutional Ethics Committee of BioMedical Research of Apollo Hospitals, Chennai (ACH−OTH-001/11-20), and it was conducted following the Helsinki guidelines. Each participant provided informed consent after signing the consent form. The urine samples were ultrafiltered (0.22 μm) and clarified by centrifuging them at 2000x g for 30 min at 4 °C within 1 h. EVs were isolated from urine using the TEI kit from Invitrogen, USA, following a previously described protocol.[73] Clarified urine was mixed with the reagent in equal proportions to achieve a clear homogeneous solution. After incubating the mixture at room temperature for an hour, it was centrifuged at 10,000*g* for 1 h at 4 °C. The EV pellet was then reconstituted in 0.01 M phosphate-buffered saline (PBS) buffer and stored at −80 °C for subsequent analysis.

Biophysical and Molecular Characterization of Isolated Urinary EVs. The experimental methods involved several techniques to characterize the UEVs including their morphology, size, concentration, and specific protein markers. UEVs were analyzed using a Jeol TEM—2100 plus microscope from Tokyo, Japan, based on the previously reported procedure.[37,74] NTA was performed following our previously reported procedures.[30]

For Western blotting, an equivalent volume of resuspended EVs was lysed in 1× radioimmunoprecipitation assay (50 mM Tris−HCl of pH 7.4, 0.25% sodium deoxycholate, 1% Nonidet P-40, 150 mM NaCl and 1 mM EDTA) buffer that contained protease inhibitor cocktail from Sigma. A bicinchoninic acid protein assay was performed to determine the protein concentration (Thermo Fisher). The proteins were resolved in 12% sodium dodecyl sulfate-polyacrylamide gel electrophoresis and then transferred to a nitrocellulose membrane (Bio-Rad). The membrane was blocked using PBS with 5% BSA and incubated 1:10 diluted Alix (3A9) mouse monoclonal antibody (mAb) (Cell Signaling Technology) overnight at 4 °C. PBS with Tween-20 (PBST) was used for three washes of membranes and were exposed to antimouse and antirabbit horseradish peroxidase (HRP)-conjugated secondary antibodies for one h at room temperature. Following three washes in 1× PBST, the blots were developed using a luminol enhancer solution provided by Bio-Rad.

SERS Substrate Preparation and Detection. *Ag Colloids Preparation.* AgNPs were synthesized by reducing silver nitrate using trisodium citrate.[75,76] A typical synthesis involves heating 50 mL of 1 mM $AgNO_3$ solution, the mixture was boiled for a time period of 20 min while adding 1 mL of 1% citrate solution in drops, and finally, the solution was cooled to room temperature using an ice bath. The prepared Ag colloid was concentrated to 50 μL (5 mL of the colloid was concentrated to 50 μL) by centrifugation. The process of colloid preparation entails the generation of a stable dispersion of nanoparticles and EVs in a solution of 1× PBS. The nanoparticle-EV dispersion was amalgamated in equal proportions. Glass slides, enveloped in aluminum foil, functioned as substrates for the colloid analyte mixture. A precise volume of this mixture (3 μL) was deposited onto the prepared slides using a drop-casting technique. Subsequently, the coated slides were dried in an oven maintained at 30 °C for 2 h. The resultant dried samples were subjected to SERS measurements.

SERS Measurements and Data Analysis. The UV−visible spectra were obtained using a multiscanner sky spectrophotometer (Thermo Scientific, USA) operated at a resolution of 1 nm. SERS spectra were recorded by using a B&W Tek portable Raman spectrometer (BWS415-785S-001; B&W Tek). While using the excitation source of 785 nm, a diode laser, with a numerical aperture of 0.65 (40× Plan objective, Olympus) and a 135 mW laser power (30%). The exposure time was 3s with 3 accumulations. Baseline correction

https://doi.org/10.1021/acsomega.5c00838
ACS Omega 2025, 10, 16874−16883

was automatically executed. For each sample measurement, three different locations were randomly selected and three substrates were measured for each condition. The uniformity and reproducibility of the SERS substrate represent critical parameters for its performance evaluation. To assess spot-to-spot reproducibility, SERS spectra were recorded at 25 distinct locations on a single substrate. To evaluate substrate-to-substrate variability, SERS spectra were collected from five spots on each of ten different substrates, yielding a total of 50 spectra. The reproducibility and reliability of the substrates were confirmed by relative standard deviation values of 7.3% and 8.9%, respectively, underscoring the consistency of the SERS responses across individual spots and different substrates shown in Figure S4. The pictorial and photographic images of the SERS substrate array are presented in Figure S5.

Statistical Analysis. IBM SPSS software version 26 was used to compare SERS spectral regions of urine EVs between individuals with DMD and age-matched controls, using independent-variable tests and one-way ANOVA, with a p-value of less than 0.01.

Machine Learning Algorithms for Spectral Analysis and Classification. We devised a prediction model and conducted an evaluation using Anaconda and Python 3.9.16 (64 bit) as well as running the Jupyter Notebook for data analysis or model creation. The data preprocessing stage entails the standardization of variables to bring them to a common denominator and reduce noise to enhance the data quality. Dimensionality reduction was performed using PCA. This technique facilitates the extraction of the primary components from the selected data set by computing the eigenvectors and eigenvalues of the covariance matrix. The principal components were identified by arranging the eigenvectors in descending order based on their corresponding eigenvalues. Subsequently, the top k eigenvectors (principal components) were selected, where k represents the desired dimensionality of the reduced data set. Our models were trained on the entire data set using k-fold cross-validation resampling to avoid overfitting. This method uses different portions of data to test and train the model across multiple iterations. This feature of the SVM and KNN comparison provided an effective area for measuring and assessing the spectral data of UEVs in DMD patients versus controls for rapid diagnosis.

■ ASSOCIATED CONTENT

Supporting Information

The Supporting Information is available free of charge at https://pubs.acs.org/doi/10.1021/acsomega.5c00838.

Raman peak assignments for UEVs from DMD and healthy controls; average SERS spectra of four DMD patients at different stages; Bar chart of phenylalanine and alpha-spectral protein levels; comparison of UEV SERS peaks with skeletal muscle proteins; statistical analysis (400−1800 cm^{-1}, $P < 0.01$); SERS substrate uniformity and reproducibility; and white light images of the SERS substrate (PDF)

■ AUTHOR INFORMATION

Corresponding Author

Raja Natesan Sella − *Membrane Protein Interaction Laboratory, Department of Genetic Engineering, School of Bioengineering, SRM Institute of Science and Technology, Chengalpattu 603 203 Tamil Nadu, India;* orcid.org/0000-0002-5495-7110; Phone: +91 9940194847; Email: rajan3@srmist.edu.in

Authors

Archana Rajavel − *Membrane Protein Interaction Laboratory, Department of Genetic Engineering, School of Bioengineering, SRM Institute of Science and Technology, Chengalpattu 603 203 Tamil Nadu, India*

Jayasree Kumar − *Raman Research Laboratory (RARE Lab), Department of Chemistry, SRM University-AP, Andhra Pradesh, Amaravati 522502, India*

Narayanan Essakipillai − *Department of Computer Applications, Faculty of Science and Humanities, SRM Institute of Science and Technology, Chengalpattu 603 203 Tamil Nadu, India*

Ramajayam Anbazhagan − *Department of Mathematics, Faculty of Engineering and Technology, SRM Institute of Science and Technology, Chengalpattu 603 203 Tamil Nadu, India*

Rajapandiyan Panneerselvam − *Raman Research Laboratory (RARE Lab), Department of Chemistry, SRM University-AP, Andhra Pradesh, Amaravati 522502, India;* orcid.org/0000-0002-3566-4558

Jayashree Ramakrishnan − *Department of Computer Applications, Faculty of Science and Humanities, SRM Institute of Science and Technology, Chengalpattu 603 203 Tamil Nadu, India*

Viswanathan Venkataraman − *Department of Paediatrics Neurology, Apollo Children's Hospital, Chennai 600 006 Tamil Nadu, India*

Complete contact information is available at: https://pubs.acs.org/10.1021/acsomega.5c00838

Author Contributions

#J.K. and N.E. contributed equally. Conceptualization and design, N.S.R., A.R.; Data Acquisition, J.K., A.R.; Data curation, A.R., N.E.; Investigation, R.P.; A.R.; Supervision, N.S.R.; Validation, N.E., A.R.; Methodology, N.S.R., A.R.; Project Administration, N.S.R., R.P.; Formal Analysis, N.E.; Software J.R.; Visualization, N.E.; Resources, V.V., J.P.R.; Writing—Original draft A.R.; Writing—Review & Editing N.S.R., A.R.

Funding

This research did not receive any specific grants from funding agencies in the public, commercial, or not-for-profit sectors.

Notes

The authors declare no competing financial interest.

■ ACKNOWLEDGMENTS

The first author acknowledges the SRM IST for the fellowship support. We acknowledge staff members of the Apollo Children's Hospital for their assistance in collecting urine samples from DMD children. We also thank the children and their parents who participated in this study.

■ REFERENCES

(1) Birnkrant, D. J.; Bushby, K.; Bann, C. M.; Apkon, S. D.; Blackwell, A.; Brumbaugh, D.; Case, L. E.; Clemens, P. R.; Hadjiyannakis, S.; Pandya, S.; Street, N.; Tomezsko, J.; Wagner, K. R.; Ward, L. M.; Weber, D. R. Diagnosis and Management of Duchenne Muscular Dystrophy, Part 1: Diagnosis, and Neuromuscular, Rehabilitation, Endocrine, and Gastrointestinal and Nutritional Management. *Lancet Neurol.* **2018**, *17* (3), 251−267.

(2) Tyler, K. L. Origins and Early Descriptions of "Duchenne Muscular Dystrophy.". *Muscle Nerve* **2003**, *28* (4), 402−422.
(3) Birnkrant, D. J.; Bushby, K.; Bann, C. M.; Alman, B. A.; Apkon, S. D.; Blackwell, A.; Case, L. E.; Cripe, L.; Hadjiyannakis, S.; Olson, A. K.; Sheehan, D. W.; Bolen, J.; Weber, D. R.; Ward, L. M. Diagnosis and Management of Duchenne Muscular Dystrophy, Part 2: Respiratory, Cardiac, Bone Health, and Orthopaedic Management. *Lancet Neurol.* **2018**, *17* (4), 347−361.
(4) Verhaart, I. E. C.; Johnson, A.; Thakrar, S.; Vroom, E.; De Angelis, F.; Muntoni, F.; Aartsma-Rus, A. M.; Niks, E. H. Muscle Biopsies in Clinical Trials for Duchenne Muscular Dystrophy − Patients' and Caregivers' Perspective. *Neuromuscular Disord.* **2019**, *29* (8), 576−584.
(5) Chamberlain, J. C.; Chamberlain, J. R.; et al. Diagnosis of Duchenne and Becker Muscular Dystrophies by Polymerase Chain Reaction. A Multicenter Study. *JAMA* **1992**, *267* (19), 2609−2615.
(6) Singh, R.; Vijjaya; Kabra, M. Multiplex PCR for Rapid Detection of Exonal Deletions in Patients of Duchenne Muscular Dystrophy. *Indian J. Clin. Biochem.* **2006**, *21* (1), 147.
(7) Percy, M. E.; Andrews, D. F.; Thompson, M. W. Serum Creatine Kinase in the Detection of Duchenne Muscular Dystrophy Carriers: Effects of Season and Multiple Testing. *Muscle Nerve* **1982**, *5* (1), 58−64.
(8) Wong, S. H.; McClaren, B. J.; Archibald, A. D.; Weeks, A.; Langmaid, T.; Ryan, M. M.; Kornberg, A.; Metcalfe, S. A. A Mixed Methods Study of Age at Diagnosis and Diagnostic Odyssey for Duchenne Muscular Dystrophy. *Eur. J. Hum. Genet.* **2015**, *23* (10), 1294−1300.
(9) Aartsma-Rus, A.; Ginjaar, I. B.; Bushby, K. The Importance of Genetic Diagnosis for Duchenne Muscular Dystrophy. *J. Med. Genet.* **2016**, *53* (3), 145−151.
(10) Schwartz, C. E.; Stark, R. B.; Audhya, I. F.; Gooch, K. L. Characterizing the Quality-of-Life Impact of Duchenne Muscular Dystrophy on Caregivers: A Case-Control Investigation. *J. Patient Rep. Outcomes* **2021**, *5* (1), 124.
(11) Hathout, Y.; Brody, E.; Clemens, P. R.; Cripe, L.; DeLisle, R. K.; Furlong, P.; Gordish-Dressman, H.; Hache, L.; Henricson, E.; Hoffman, E. P.; Kobayashi, Y. M.; Lorts, A.; Mah, J. K.; McDonald, C.; Mehler, B.; Nelson, S.; Nikrad, M.; Singer, B.; Steele, F.; Sterling, D.; Sweeney, H. L.; Williams, S.; Gold, L. Large-Scale Serum Protein Biomarker Discovery in Duchenne Muscular Dystrophy. *Proc. Natl. Acad. Sci. U.S.A.* **2015**, *112* (23), 7153−7158.
(12) Kohler, M.; Clarenbach, C. F.; Böni, L.; Brack, T.; Russi, E. W.; Bloch, K. E. Quality of Life, Physical Disability, and Respiratory Impairment in Duchenne Muscular Dystrophy. *Am. J. Respir. Crit. Care Med.* **2005**, *172* (8), 1032−1036.
(13) Ryder, S.; Leadley, R. M.; Armstrong, N.; Westwood, M.; de Kock, S.; Butt, T.; Jain, M.; Kleijnen, J. The Burden, Epidemiology, Costs and Treatment for Duchenne Muscular Dystrophy: An Evidence Review. *Orphanet J. Rare Dis* **2017**, *12* (1), 79.
(14) Théry, C. Exosomes: Secreted Vesicles and Intercellular Communications. *F1000 Biol. Rep.* **2011**, *3* (1), 15.
(15) Mathivanan, S.; Ji, H.; Simpson, R. J. Exosomes: Extracellular Organelles Important in Intercellular Communication. *J. Proteomics* **2010**, *73* (10), 1907−1920.
(16) Wu, X.; Zheng, T.; Zhang, B. Exosomes in Parkinson's Disease. *Neurosci. Bull.* **2017**, *33*, 331−338. Science Press June
(17) Salem, K. Z.; Moschetta, M.; et al. Exosomes in Tumor Angiogenesis. *Methods Mol. Biol.* **2016**, *1464*, 25−34.
(18) Howitt, J.; Hill, A. F. Exosomes in the Pathology of Neurodegenerative Diseases. *J. Biol. Chem.* **2016**, *291* (52), 26589−26597.
(19) Liu, W.; Bai, X.; Zhang, A.; Huang, J.; Xu, S.; Zhang, J. Role of Exosomes in Central Nervous System Diseases. *Front. Mol. Neurosci.* **2019**, *12*, 240.
(20) Wong, C.-H.; Chen, Y.-C. Clinical Significance of Exosomes as Potential Biomarkers in Cancer. *World J. Clin. Cases* **2019**, *7* (2), 171.
(21) Haney, M. J.; Klyachko, N. L.; Zhao, Y.; Gupta, R.; Plotnikova, E. G.; He, Z.; Patel, T.; Piroyan, A.; Sokolsky, M.; Kabanov, A. V.; Batrakova, E. V. Exosomes as Drug Delivery Vehicles for Parkinson's Disease Therapy. *J. Controlled Release* **2015**, *207*, 18−30.
(22) Palaniswamy, R.; Sevugan, K.; Sampathkumar Srisharnitha, A. Molecular Signatures in Exosomes as Diagnostic Markers for Neurodegenerative Disorders. *Annals of Alzheimer's and Dementia Care* **2020**, *4* (1), 012−017.
(23) Blaschke, C. R. K.; Hartig, J. P.; Grimsley, G.; Liu, L.; Semmes, O. J.; Wu, J. D.; Ippolito, J. E.; Hughes-Halbert, C.; Nyalwidhe, J. O.; Drake, R. R. Direct N-Glycosylation Profiling of Urine and Prostatic Fluid Glycoproteins and Extracellular Vesicles. *Front. Chem.* **2021**, *9*, 734280.
(24) Monteleone, M. C.; Billi, S. C.; Viale, L.; Catoira, N. P.; Frasch, A. C.; Brocco, M. A. Search of Brain-Enriched Proteins in Salivary Extracellular Vesicles for Their Use as Mental Disease Biomarkers: A Pilot Study of the Neuronal Glycoprotein M6a. *J. Affect Disord. Rep* **2020**, *1*, 100003.
(25) Kupcova Skalnikova, H.; Bohuslavova, B.; Turnovcova, K.; Juhasova, J.; Juhas, S.; Rodinova, M.; Vodicka, P. Isolation and Characterization of Small Extracellular Vesicles from Porcine Blood Plasma, Cerebrospinal Fluid, and Seminal Plasma. *Proteomes* **2019**, *7* (2), 17.
(26) Wang, S.; Kojima, K.; Mobley, J. A.; West, A. B. Proteomic Analysis of Urinary Extracellular Vesicles Reveal Biomarkers for Neurologic Disease. *EBioMedicine* **2019**, *45*, 351−361.
(27) Boukouris, S.; Mathivanan, S. Exosomes in Bodily Fluids Are a Highly Stable Resource of Disease Biomarkers. *Proteomics Clin. Appl.* **2015**, *9* (3−4), 358−367.
(28) Newman, L. A.; Muller, K.; Rowland, A. Circulating Cell-Specific Extracellular Vesicles as Biomarkers for the Diagnosis and Monitoring of Chronic Liver Diseases. *Cell. Mol. Life Sci.* **2022**, *79* (5), 232.
(29) Winston, C. N.; Sukreet, S.; Lynch, H.; Lee, V. M. Y.; Wilcock, D. M.; Nelson, P. T.; Rissman, R. A. Evaluation of Blood-Based Exosomes as Biomarkers for Aging-Related TDP-43 Pathology. DOI: .
(30) Rajavel, A.; Essakipillai, N.; Anbazhagan, R.; Ramakrishnan, J.; Venkataraman, V.; Natesan Sella, R. Molecular Profiling of Blood Plasma-Derived Extracellular Vesicles Derived from Duchenne Muscular Dystrophy Patients through Integration of FTIR Spectroscopy and Machine Learning Reveals Disease Signatures. *Spectrochim. Acta, Part A* **2025**, *326*, 125236.
(31) Cui, X.; Zhao, Z.; Zhang, G.; Chen, S.; Zhao, Y.; Lu, J. Analysis and Classification of Kidney Stones Based on Raman Spectroscopy. *Biomed. Opt. Express* **2018**, *9* (9), 4175−4183.
(32) Soares Martins, T.; Magalhães, S.; Rosa, I. M.; Vogelgsang, J.; Wiltfang, J.; Delgadillo, I.; Catita, J.; da Cruz e Silva, O. A. B.; Nunes, A.; Henriques, A. G. Potential of FTIR Spectroscopy Applied to Exosomes for Alzheimer's Disease Discrimination: A Pilot Study. *Am. J. Alzheimer's Dis.* **2020**, *74* (1), 391−405.
(33) Stępień, E. Ł.; Kamińska, A.; Surman, M.; Karbowska, D.; Wróbel, A.; Przybyło, M. Fourier-Transform InfraRed (FT-IR) Spectroscopy to Show Alterations in Molecular Composition of EV Subpopulations from Melanoma Cell Lines in Different Malignancy. *Biochem. Biophys. Rep.* **2021**, *25*, 100888.
(34) Jalaludin, I.; Lubman, D. M.; Kim, J. MALDI-MS: A Powerful but Underutilized Mass Spectrometric Technique for Exosome Research. *Mass Spectrom. Lett.* **2021**, *12* (3), 93−105.
(35) Yu, Z.; Zhao, C.; Hu, S.; Zhang, H.; Li, W.; Zhang, R.; Luo, Q.; Yang, H. MALDI-MS-Based Biomarker Analysis of Extracellular Vesicles from Human Lung Carcinoma Cells. *RSC Adv.* **2021**, *11* (41), 25375−25380.
(36) Yu, Z.; Zhao, C.; Hu, S.; Zhang, H.; Li, W.; Zhang, R.; Luo, Q.; Yang, H. MALDI-MS-Based Biomarker Analysis of Extracellular Vesicles from Human Lung Carcinoma Cells. *RSC Adv.* **2021**, *11* (41), 25375−25380.
(37) Rajavel, A. Identification of Extracellular Vesicles Derived from Plasma Using MALDI-TOF MS: Influence of Operating Conditions. *J. Appl. Biotechnol. Rep.* **2023**, *10* (3), 1098−1108.
(38) Singhto, N.; Vinaiphat, A.; Thongboonkerd, V. RETRACTED ARTICLE: Discrimination of urinary exosomes from microvesicles by

https://doi.org/10.1021/acsomega.5c00838
ACS Omega 2025, 10, 16874−16883

lipidomics using thin layer liquid chromatography (TLC) coupled with MALDI-TOF mass spectrometry. *Sci. Rep.* **2019**, *9* (1), 13834.
(39) Kerr, L. T.; Gubbins, L.; Weiner Gorzel, K.; Sharma, S.; Kell, M.; McCann, A.; Hennelly, B. M. Raman Spectroscopy and SERS Analysis of Ovarian Tumour Derived Exosomes (TEXs): A Preliminary Study. In *Biophotonics: Photonic Solutions for Better Health Care IV*; SPIE, 2014; Vol. *9129*, p 91292Q..
(40) Zong, C.; Xu, M.; Xu, L.-J.; Wei, T.; Ma, X.; Zheng, X.-S.; Hu, R.; Ren, B. Surface-Enhanced Raman Spectroscopy for Bioanalysis: Reliability and Challenges. *Chem. Rev.* **2018**, *118* (10), 4946−4980.
(41) Lu, D.; Zhang, B.; Shangguan, Z.; Lu, Y.; Chen, J.; Huang, Z. Machine Learning-Based Exosome Profiling of Multi-Receptor SERS Sensors for Differentiating Adenocarcinoma in Situ from Early-Stage Invasive Adenocarcinoma. *Colloids Surf., B* **2024**, *236*, 113824.
(42) Diao, X.; Li, X.; Hou, S.; Li, H.; Qi, G.; Jin, Y. Machine Learning-Based Label-Free SERS Profiling of Exosomes for Accurate Fuzzy Diagnosis of Cancer and Dynamic Monitoring of Drug Therapeutic Processes. *Anal. Chem.* **2023**, *95* (19), 7552−7559.
(43) Choi, N.; Schlücker, S. Convergence of Surface-Enhanced Raman Scattering with Molecular Diagnostics: A Perspective on Future Directions. *ACS Nano* **2024**, *18* (8), 5998−6007.
(44) Ralbovsky, N. M.; Dey, P.; Galfano, A.; Dey, B. K.; Lednev, I. K. A Novel Method for Detecting Duchenne Muscular Dystrophy in Blood Serum of Mdx Mice. *Genes* **2022**, *13* (8), 1342.
(45) Ralbovsky, N. M.; Dey, P.; Galfano, A.; Dey, B. K.; Lednev, I. K. Diagnosis of a Model of Duchenne Muscular Dystrophy in Blood Serum of Mdx Mice Using Raman Hyperspectroscopy. *Sci. Rep.* **2020**, *10* (1), 11734.
(46) Ju, J.; Hsieh, C.-M.; Tian, Y.; Kang, J.; Chia, R.; Chang, H.; Bai, Y.; Xu, C.; Wang, X.; Liu, Q. Surface Enhanced Raman Spectroscopy Based Biosensor with a Microneedle Array for Minimally Invasive *In Vivo* Glucose Measurements. *ACS Sens.* **2020**, *5* (6), 1777−1785.
(47) Qi, Y.; Hu, D.; Jiang, Y.; Wu, Z.; Zheng, M.; Chen, E. X.; Liang, Y.; Sadi, M. A.; Zhang, K.; Chen, Y. P. Recent Progresses in Machine Learning Assisted Raman Spectroscopy. *Adv. Opt. Mater.* **2023**, *11* (14), 2203104.
(48) Zhang, Z.; Jiang, S.; Wang, X.; Dong, T.; Wang, Y.; Li, D.; Gao, X.; Qu, Z.; Li, Y. A Novel Enhanced Substrate for Label-Free Detection of SARS-CoV-2 Based on Surface-Enhanced Raman Scattering. *Sens. Actuators, B* **2022**, *359*, 131568.
(49) Živanović, V.; Seifert, S.; Drescher, D.; Schrade, P.; Werner, S.; Guttmann, P.; Szekeres, G. P.; Bachmann, S.; Schneider, G.; Arenz, C.; Kneipp, J. Optical Nanosensing of Lipid Accumulation Due to Enzyme Inhibition in Live Cells. *ACS Nano* **2019**, *13* (8), 9363−9375.
(50) Shi, J.; Li, R.; Wang, Y.; Zhang, C.; Lyu, X.; Wan, Y.; Yu, Z. Detection of Lung Cancer through SERS Analysis of Serum. *Spectrochim. Acta, Part A* **2024**, *314*, 124189.
(51) Woo, H.; Park, J.; Kim, K. H.; Ku, J. Y.; Ha, H. K.; Cho, Y. Alix-normalized Exosomal Programmed Death-ligand 1 Analysis in Urine Enables Precision Monitoring of Urothelial Cancer. *Cancer Sci.* **2024**, *115* (5), 1602−1610.
(52) Stamplecoskie, K. G.; Scaiano, J. C.; Tiwari, V. S.; Anis, H. Optimal Size of Silver Nanoparticles for Surface-Enhanced Raman Spectroscopy. *J. Phys. Chem. C* **2011**, *115* (5), 1403−1409.
(53) Schill, K. E.; Altenberger, A. R.; Lowe, J.; Periasamy, M.; Villamena, F. A.; Rafael-Fortney, J. A.; Devor, S. T. Muscle Damage, Metabolism, and Oxidative Stress in *Mdx* Mice: Impact of Aerobic Running. *Muscle Nerve* **2016**, *54* (1), 110−117.
(54) Plesia, M.; Stevens, O. A.; Lloyd, G. R.; Kendall, C. A.; Coldicott, I.; Kennerley, A. J.; Miller, G.; Shaw, P. J.; Mead, R. J.; Day, J. C. C.; Alix, J. J. P. *In Vivo* Fiber Optic Raman Spectroscopy of Muscle in Preclinical Models of Amyotrophic Lateral Sclerosis and Duchenne Muscular Dystrophy. *ACS Chem. Neurosci.* **2021**, *12* (10), 1768−1776.
(55) Vieira, N. M.; Spinazzola, J. M.; Alexander, M. S.; Moreira, Y. B.; Kawahara, G.; Gibbs, D. E.; Mead, L. C.; Verjovski-Almeida, S.; Zatz, M.; Kunkel, L. M. Repression of Phosphatidylinositol Transfer Protein α Ameliorates the Pathology of Duchenne Muscular Dystrophy. *Proc. Natl. Acad. Sci. U.S.A.* **2017**, *114* (23), 6080−6085.
(56) Batra, A.; Lott, D. J.; Willcocks, R.; Forbes, S. C.; Triplett, W.; Dastgir, J.; Yun, P.; Reghan Foley, A.; Bönnemann, C. G.; Vandenborne, K.; Walter, G. A. Lower Extremity Muscle Involvement in the Intermediate and Bethlem Myopathy Forms of COL6-Related Dystrophy and Duchenne Muscular Dystrophy: A Cross-Sectional Study. *J. Neuromuscul. Dis.* **2020**, *7* (4), 407−417.
(57) Suárez-Calvet, X.; Fernández-Simón, E.; Natera, D.; Jou, C.; Pinol-Jurado, P.; Villalobos, E.; Ortez, C.; Monceau, A.; Schiava, M.; Codina, A.; Verdu-Díaz, J.; Clark, J.; Laidler, Z.; Mehra, P.; Gokul-Nath, R.; Alonso-Perez, J.; Marini-Bettolo, C.; Tasca, G.; Straub, V.; Guglieri, M.; Nascimento, A.; Diaz-Manera, J. Decoding the Transcriptome of Duchenne Muscular Dystrophy to the Single Nuclei Level Reveals Clinical-Genetic Correlations. *Cell Death Dis.* **2023**, *14* (9), 596.
(58) Nguyen, T. T.; Gobinet, C.; Feru, J.; Pasco, S. B.; Manfait, M.; Piot, O. Characterization of Type I and IV Collagens by Raman Microspectroscopy: Identification of Spectral Markers of the Dermo-Epidermal Junction. *J. Spectrosc.* **2012**, *27* (5−6), 421−427.
(59) Sahani, R.; Wallace, C. H.; Jones, B. K.; Blemker, S. S. Diaphragm Muscle Fibrosis Involves Changes in Collagen Organization with Mechanical Implications in Duchenne Muscular Dystrophy. *J. Appl. Physiol.* **2022**, *132* (3), 653−672.
(60) Kharraz, Y.; Guerra, J.; Pessina, P.; Serrano, A. L.; Muñoz-Cánoves, P. Understanding the Process of Fibrosis in Duchenne Muscular Dystrophy. *Biomed. Res. Int.* **2014**, *2014*, 1−11.
(61) Bertorini, T. E.; Palmieri, G. M. A.; Airozo, D.; Edwards, N. L.; Fox, I. H. Increased Adenine Nucleotide Turnover in Duchenne Muscular Dystrophy. *Pediatr. Res.* **1981**, *15* (12), 1478−1482.
(62) Frass, M.; Toifl, K.; Leixnering, W. Adenine Metabolism in Erythrocytes of Patients with Duchenne Muscular Dystrophy. *Eur. Neurol.* **2004**, *22* (5), 380−384.
(63) Willers, I.; Singh, S.; Goedde, H. W. Purine Metabolism in Fibroblasts of Patients with Duchenne& Rsquo;s Muscular Dystrophy. *Hum. Hered.* **1982**, *32* (4), 233−239.
(64) Lynge, J.; Juel, C.; Hellsten, Y. Extracellular Formation and Uptake of Adenosine during Skeletal Muscle Contraction in the Rat: Role of Adenosine Transporters. *J. Physiol.* **2001**, *537* (2), 597−605.
(65) Ryu, S.-M.; Koo, T.; Kim, K.; Lim, K.; Baek, G.; Kim, S.-T.; Kim, H. S.; Kim, D.; Lee, H.; Chung, E.; Kim, J.-S. Adenine Base Editing in Mouse Embryos and an Adult Mouse Model of Duchenne Muscular Dystrophy. *Nat. Biotechnol.* **2018**, *36* (6), 536−539.
(66) Chemello, F.; Chai, A. C.; Li, H.; Rodriguez-Caycedo, C.; Sanchez-Ortiz, E.; Atmanli, A.; Mireault, A. A.; Liu, N.; Bassel-Duby, R.; Olson, E. N. Precise Correction of Duchenne Muscular Dystrophy Exon Deletion Mutations by Base and Prime Editing. *Sci. Adv.* **2021**, *7* (18), No. eabg4910.
(67) Almeida-Becerril, T.; Rodríguez-Cruz, M.; Villa-Morales, J.; Sánchez-Mendoza, C. R.; Galeazzi-Aguilar, J. E. Circulating Nrf2, Glutathione, and Malondialdehyde Correlate with Disease Severity in Duchenne Muscular Dystrophy. *Antioxidants* **2023**, *12* (4), 871.
(68) Carmen, L.; Maria, V.; Morales-Medina, J. C.; Vallelunga, A.; Palmieri, B.; Iannitti, T. Role of Proteoglycans and Glycosaminoglycans in Duchenne Muscular Dystrophy. *Glycobiology* **2019**, *29* (2), 110−123.
(69) Czibik, G.; Mezdari, Z.; Murat Altintas, D.; Bréhat, J.; Pini, M.; d'Humières, T.; Delmont, T.; Radu, C.; Breau, M.; Liang, H.; Martel, C.; Abatan, A.; Sarwar, R.; Marion, O.; Naushad, S.; Zhang, Y.; Halfaoui, M.; Suffee, N.; Morin, D.; Adnot, S.; Hatem, S.; Yavari, A.; Sawaki, D.; Derumeaux, G. Dysregulated Phenylalanine Catabolism Plays a Key Role in the Trajectory of Cardiac Aging. *Circulation* **2021**, *144* (7), 559−574.
(70) Radley-Crabb, H. G.; Marini, J. C.; Sosa, H. A.; Castillo, L. I.; Grounds, M. D.; Fiorotto, M. L. Dystropathology Increases Energy Expenditure and Protein Turnover in the Mdx Mouse Model of Duchenne Muscular Dystrophy. *PLoS One* **2014**, *9* (2), No. e89277.
(71) Wu, G.; Bazer, F. W.; Burghardt, R. C.; Johnson, G. A.; Kim, S. W.; Knabe, D. A.; Li, P.; Li, X.; McKnight, J. R.; Satterfield, M. C.;

https://doi.org/10.1021/acsomega.5c00838
ACS Omega 2025, 10, 16874−16883

Spencer, T. E. Proline and Hydroxyproline Metabolism: Implications for Animal and Human Nutrition. *Amino Acids* **2011**, *40* (4), 1053−1063.
(72) Berkemeier, F.; Bertz, M.; Xiao, S.; Pinotsis, N.; Wilmanns, M.; Gräter, F.; Rief, M. Fast-Folding α-Helices as Reversible Strain Absorbers in the Muscle Protein Myomesin. *Proc. Natl. Acad. Sci. U.S.A.* **2011**, *108* (34), 14139−14144.
(73) Patel, G. K.; Khan, M. A.; Zubair, H.; Srivastava, S. K.; Khushman, M.; Singh, S.; Singh, A. P. Comparative Analysis of Exosome Isolation Methods Using Culture Supernatant for Optimum Yield, Purity and Downstream Applications. *Sci. Rep.* **2019**, *9* (1), 5335.
(74) Dash, M.; Palaniyandi, K.; Ramalingam, S.; Sahabudeen, S.; Raja, N. S. Exosomes Isolated from Two Different Cell Lines Using Three Different Isolation Techniques Show Variation in Physical and Molecular Characteristics. *Biochim. Biophys. Acta, Biomembr.* **2021**, *1863* (2), 183490.
(75) Munro, C. H.; Smith, W. E.; Garner, M.; Clarkson, J.; White, P. C. Characterization of the Surface of a Citrate-Reduced Colloid Optimized for Use as a Substrate for Surface-Enhanced Resonance Raman Scattering. *Langmuir* **1995**, *11* (10), 3712−3720.
(76) Lee, P. C.; Meisel, D. Adsorption and Surface-Enhanced Raman of Dyes on Silver and Gold Sols. *J. Phys. Chem.* **1982**, *86* (17), 3391−3395.

https://doi.org/10.1021/acsomega.5c00838
ACS Omega 2025, 10, 16874−16883